ORIGINAL ARTICLE

Defactinib attenuates osteoarthritis by inhibiting positive feedback loop between H-type vessels and MSCs in subchondral bone

Yanjun Hu [a,c,1], Hangtian Wu [a,c,1], Ting Xu [d,1], Yutian Wang [a,c], Hanjun Qin [a,c], Zilong Yao [a,c], Peisheng Chen [a,e], Yongheng Xie [a,c], Zhiguo Ji [a,c], Kaifan Yang [a,c], Yu Chai [a,b], Xianrong Zhang [a,c], Bin Yu [a,c,**], Zhuang Cui [a,c,*]

[a] Department of Orthopedics, Nanfang Hospital, Southern Medical University, Guangzhou, Guangdong 510515, China
[b] Department of Orthopedic Surgery, Institute for Cell Engineering, Johns Hopkins University, Baltimore, MD 21205, USA
[c] Key Laboratory of Bone and Cartilage Regeneration Medicine, Southern Medical University, Guangzhou, Guangdong 510515, China
[d] Department of Sleep Medicine Center, Nanfang Hospital, Southern Medical University, Guangzhou, Guangdong 510515, China
[e] Department of Orthopedics, Fuzhou Second Hospital Affiliated to Xiamen University, Fuzhou, Fujian 350007, China

ARTICLE INFO

SUMMARY

Background: Abnormal bone formation in subchondral bone resulting from uncoupled bone remodeling is considered a central feature in osteoarthritis (OA) pathogenesis. H-type vessels can couple angiogenesis and osteogenesis. We previously revealed that elevated H-type vessels in subchondral bone were correlated with OA and focal adhesion kinase (FAK) in MSCs is critical for H-type vessel formation in osteoporosis. The aim of this study was to explore the correlation between H-type vessels and MSCs in OA pathogenesis through regulation of H-type vessel formation using defactinib (an FAK inhibitor).
Methods: In vivo: 3-month-old male C57BL/6J (WT) mice were randomly divided into three groups: sham controls, vehicle-treated ACLT mice, and defactinib-treated ACLT mice (25 mg/kg, intraperitoneally weekly). *In vitro:* we explored the role of conditioned medium (CM) of MSCs from subchondral bone of different groups on the angiogenesis of endothelial cells (ECs). Flow cytometry, Western blotting, ELISA, real time (RT)-PCR, immuno-staining, CT-based microangiography, and bone micro-CT (μCT) were used to detect changes in relative cells and tissues.
Results: This study demonstrated that inhibition of H-type vessels with defactinib alleviated OA by inhibiting H-type vessel-linked MSCs in subchondral bone. During OA pathogenesis, H-type vessels and MSCs formed a positive feedback loop contributing to abnormal bone formation in subchondral bone. Elevated H-type vessels provided indispensable MSCs for abnormal bone formation in subchondral bone. Flow cytometry and immunostaining results confirmed that the amount of MSCs in subchondral bone was obviously higher in vehicle-treated ACLT mice than that in sham controls and defactinib-treated ACLT mice. *In vitro*, p-FAK in MSCs from subchondral bone of vehicle-treated ALCT mice increased significantly relative to other groups. Further, the CM from MSCs of vehicle-treated ACLT mice enhanced angiogenesis of ECs through FAK-Grb2-MAPK-linked VEGF expression.
Conclusions: Our results demonstrate that defactinib inhibits OA by suppressing the positive feedback loop between H-type vessels and MSCs in subchondral bone.
The translational potential of this article: Our results provide a mechanistic rationale for the use of defactinib as an effective candidate for OA treatment.

Introduction

Osteoarthritis (OA), characterized by subchondral bone sclerosis, osteophyte formation, and elevated cartilage degradation, is the most common multifactorial degenerative joint disorder [1], with millions affected worldwide [2]. Currently, the exact etiology of OA remains

---

unclear [3,4], and there are no effective disease-modifying therapies for OA.

Although articular cartilage degeneration is the main characteristic of OA, the whole joint is involved during the progression of OA [5–8]. Of note, abnormal bone formation in subchondral bone is considered a central feature in OA initiation and progression [9,10]. Abnormal bone formation results from erroneous mobilization and recruitment of mesenchymal stem cells (MSCs) following increased and uncoupled bone remodeling in subchondral bone [9,11,12]. Specifically, after acute injury causing joint instability, such as anterior cruciate ligament (ACL) damage, over-activated osteoclasts in subchondral bone resorb excessive bone and liberate excessive factors embedded in the bone matrix, which generates an aberrant bone marrow environment leading to erroneous MSCs recruitment to bone marrow cavities or non-bone resorption sites but not to the bone resorption pits. We previously found that MSCs accumulated and were dispersed throughout the bone marrow during the onset of OA [13]. However, the origin of elevated MSCs in subchondral bone is still unknown.

Adequate blood supply is critical for bone formation [14]. In addition to bone modeling associated with bone growth, capillaries are also present at bone remodeling sites to orchestrate bone resorption and bone formation [15]. A specific vessel subtype was recently identified called H-type vessels (CD31^{hi}Emcn^{hi}) [16,17]. This new capillary can regulate perivascular osteoprogenitor recruitment and differentiation coupling angiogenesis with osteogenesis. We previously reported that the expression of H-type vessels in subchondral bone increased during the onset of OA [13].

MSC stabilization of newly formed tubes is critical for angiogenesis [18,19]. The interaction of MSCs with endothelial cells promotes blood vessel formation by secretion of angiogenic growth factors and other signaling molecules [20,21]. We previously reported that activation of FAK signaling in MSCs enhanced H-type vessel formation in cortical bone to ameliorate osteoporosis [22]. Moreover, FAK signaling can modulate angiogenesis through FAK-Grb2-MAPK-linked VEGF expression [23,24]. Therefore, we hypothesized that H-type vessels might harbor a reserve of MSCs that might be integral to the origin of MSCs necessary for abnormal bone formation in subchondral bone during OA progression, and MSCs in turn enhance angiogenesis through the FAK-Grb2-MAPK pathway to form a positive feedback loop with H-type vessels. Thus, defactinib, a FAK inhibitor, might attenuate OA by inhibiting H-type vessel-linked MSCs indispensable to abnormal bone formation in subchondral bone.

In this study, we explored *in vivo* whether treatment with defactinib could inhibit H-type vessel-linked MSCs integral to abnormal bone formation in subchondral bone and then protect articular cartilage from degeneration. *In vitro*, we examined the effect of MSCs from subchondral bone of different groups on the angiogenesis of endothelial cells (ECs) and the potential molecular mechanisms.

Materials and methods

Animals and OA model

Three-month-old male C57BL/6J (WT) mice (n = 120 total) were purchased from the animal center at Southern Medical University. Anterior cruciate ligament transection (ACLT) was done to induce abnormal mechanical loading-associated OA of the left knee. A sham operation was conducted by opening the joint capsule and then suturing the incision in the left knee of independent rodents. We randomly divided the mice into three groups: sham controls, vehicle-treated ACLT mice (solvents of defactinib), and defactinib-treated ACLT mice (n = 10 per group). Defactinib (HY-12289, MCE) was administered intraperitoneally weekly (25 mg/kg) [25]. The 30 mice were euthanized one month after surgery for micro-CT analysis and histological staining of subchondral bone and articular cartilage. An additional 90 mice were used for the following individual experiments (with the same grouping strategy and sample collection time): MSC sorting (n = 5 per group),

acquisition of conditioned medium (CM) of MSCs from subchondral bone (n = 5 per group), CT-based microangiography (n = 5 per group), calcein double-labeling experiments (n = 5 per group), qRT-PCR to detect p-FAK changes in the subchondral bone (n = 5 per group), and ELISA to detect VEGF changes in the subchondral bone and blood (n = 5 per group). All of the mice were housed in the animal facility at Southern Medical University. The experimental protocols were reviewed and approved by the Institutional Animal Care and Use Committee of the Southern Medical University.

Histochemistry, immunohistochemistry, and histomorphometry analysis

The knee joints of the mice were dissected, fixed in 4% buffered formalin for 48 h, and decalcified in 10% EDTA (pH 7.4) for four weeks. The specimens were embedded in either paraffin or optimal cutting temperature (OCT) compound (Sakura Finetek) (IF staining). Four-μm-thick longitudinally oriented sections of the knee joint medial compartment were cut and processed for H&E, Safranin O, and fast green staining. Hyaline cartilage was separated from calcified cartilage by the tidemark line. We measured the distance from the tidemark to the subchondral bone plate (SBP) as the thickness of the calcified cartilage. We also measured the distance from the tidemark to the articular cartilage surface as the thickness of the hyaline cartilage. Sagittal sections of the knee joint medial compartment were incubated with primary antibodies against CD31 (1:100, ab222783, Abcam, Cambridge, UK), endomucin (1:50, sc-65495, Santa Cruz Biotechnology, Heidelberg, Germany), Osterix (1:100, sc-393060, Santa Cruz, Biotechnology, Heidelberg, Germany), p-FAK (1:50, sc-374668, Santa Cruz, Biotechnology, Heidelberg, Germany), nestin (1:100, 66259-1-lg, Proteintech, Wuhan, China), CD146 (1:200, GTX108777, GeneTex, Shenzhen, China), MMP13 (1:100, ab39012, Abcam, Cambridge, UK), Col II (1:50, sc-52658, Santa Cruz, Biotechnology, Heidelberg, Germany), aggrecan (1:50, sc-166951, Santa Cruz, Biotechnology, Heidelberg, Germany) and ADAMTS5 (1:100,#C04789, SAB, Baltimore, USA) at 4°C overnight. For immunofluorescence staining, second antibodies conjugated with fluorescence were incubated for 1 h at room temperature (RT) while avoiding light. Next, we microphotographed the slices to perform histomorphometric measurements on the entire area of the tibia subchondral bone (Olympus DP71). Quantitative analysis was conducted in a blinded fashion with ImageJ software (v1.51j8). We counted the number of positively stained cells in the whole tibia subchondral bone area per specimen and measured five sequential specimens per mouse in each group. Osteoarthritis Research Society International-modified Mankin criteria (OARSI) scores were calculated as previously described [26].

Hard-tissue slicing and calcein double-labeling experiments

The fluorescent calcein binding dyes xylenol orange and calcein green were used to sequentially label new bone deposition and bone remodeling in subchondral bone. Xylenol orange (Sigma, 90 mg/kg) and calcein green (Sigma, 15 mg/kg) were injected subcutaneously at 10 days and 2 days, respectively, before the mice were euthanized. We then microphotographed slices to perform histomorphometric measurements on the entire area of the tibia subchondral bone.

Micro-CT analysis

We acquired the knee joints of the mice and dissected them free of soft tissue and fixed them in 70% ethanol overnight. Next, we scanned the specimens using high-resolution micro-CT (SkyScan 1172) and reconstructed the scanned images using image reconstruction software (NRecon v1.6). The data were analyzed using data analysis software (CTAn v1.9) and three-dimensional model visualization software (μ CTVol v2.0). We set the scanner to a voltage of 50 kVp, current of 200 μA, and resolution of 5.8 μm per pixel. We chose a threshold of 50 based on visual interpretation. Three-dimensional histomorphometric analysis was

performed using longitudinal images of the tibial subchondral bone. The region of interest was defined as covering the whole tibial subchondral bone medial compartment. Three-dimensional structural parameters analyzed included bone volume/total tissue volume (BV/TV), subchondral bone plate thickness (SBP.Th), trabecular number (Tb.N), and trabecular pattern factor (Tb.Pf).

CT-based microangiography

Angiography of microfil-perfused bones was performed to image the blood vessels in the bone. After the mice were euthanized, the vascular system was flushed with 0.9% normal saline solution containing heparin sodium (100U ml-1) through a needle inserted into the left ventricle. We then pressure fixed the specimens with 10% neutral buffered formalin and washed them with heparinized saline solution. Radiopaque silicone rubber compound containing lead chromate (Microfil MV-122, Flow Tech) was then injected. The specimens were stored at 4°C overnight for contrast agent polymerization. We then dissected and harvested the mouse knee joints and soaked them in 10% neutral buffered formalin for four days to ensure complete tissue fixation. Before scanning, the specimens were decalcified in a formic acid-based solution (Cal-Ex II) for 48 h to facilitate image threshold of the vasculature from the surrounding tissues. Images were acquired using a high-resolution micro-CT imaging system (SkyScan 1172). Three-dimensional analysis was performed via data analysis software (CTAn v1.9) using longitudinal images of the tibial subchondral bone. The region of interest was defined as covering the whole tibial subchondral bone medial compartment. The scanner was set at a resolution of 9 μm isotropic voxel size. We chose a threshold of 100 based on visual interpretation of threshold two-dimensional tomograms. Three-dimensional structural parameters including vessel volume/total tissue volume (VV/TV) and vessel number (VN) were analyzed.

Flow cytometry

To detect the effect of subchondral bone MSCs on angiogenesis of ECs, MSCs were isolated from the subchondral bone of the mice in different groups following a previously described protocol [27,28]. Briefly, after tibial subchondral bones were dissected free from metaphyseal bone, we first removed the periosteum and periosteal progenitors by digesting the outer surface of the subchondral bone with a protease solution (2 mg/ml collagenase A and 2.5 mg/ml trypsin) for 20 min. Next, the subchondral bone was cut into pieces and digested for 1 h to acquire mesenchymal progenitors. After red blood cell lysis with a commercial lysing solution (BD FACS, BD Biosciences, San Jose, CA, USA), cells in the supernatant (endosteal bone marrow) were collected, washed once with culture media, passed through a cell strainer, and then either used directly for flow cytometry to detect changes in the number of MSCs in the subchondral bone or plated at 1.5×10^4/well for further culture to harvest the conditioned medium (CM). For mouse MSCs, the cell surface marker expression of CD45, CD29, Sca-1, and CD105 was identified using a Mouse Multipotent Mesenchymal Stromal Cell 4-Color Flow kit (R&D Systems, Minnesota, USA) according to the manufacturer's instructions. Flow cytometric analyses were carried out with FACSCanto II Flow Cytometer (BD Biosciences, San Jose, CA, USA). Data were analyzed using BD FACSDiva software v6.1.3 (BD Biosciences, San Jose, CA, USA).

Acquisition of conditioned medium (CM)

MSCs from the subchondral bone of the mice in the different groups were seeded into 48-well culture plates at a density of 1.5×10^4/well and cultured with minimum essential medium α (α-MEM, Mediatech, Inc.) supplemented with penicillin (100 U ml^{-1}, Sigma–Aldrich), streptomycin sulfate (100 μg ml^{-1}, Sigma–Aldrich), and 10% lot-selected fetal bovine serum (FBS, Atlanta Biologicals) at 37°C in a 5% CO2 humidified incubator. After seven days of culture, the CM of the MSCs from the sham controls, vehicle-treated ACLT mice, and defactinib-treated ACLT mice

was harvested and centrifuged at $2000 \times g$ for 10 min to collect the supernatant, which was stored at −80°C or used for downstream experiments. Proteins of cultured MSCs from different groups were harvested for Western blotting.

Tube formation assay

We plated Matrigel (BD Biosciences) in 96-well culture plates and incubated them at 37°C to polymerize for 45 min. We then seeded bone marrow endothelial cells (BMECs, JNO-19263, Guangzhou, China) onto Matrigel-coated 96-well plates at a density of 2×10^4 cells/well and cultured them in culture media with the CM of the MSCs from the sham controls, vehicle-treated ACLT mice, or defactinib-treated ACLT mice. After incubation at 37°C for 6 h, the cells were observed with an inverted microscope (Leica). All of the parameters (total tube length, total loops, and total branching points) revealing the ability of BMECs to form tubes were measured using Image-Pro Plus 6 software.

Quantitative real-time PCR (qRT-PCR) analysis

The subchondral bones dissected from proximal tibias were pulverized with a pestle and mortar prechilled in liquid nitrogen. The bone particles were homogenized in TRIzol reagent (Invitrogen, Carlsbad, CA, USA) and the total RNA was harvested following the manufacturer's instructions. cDNA was synthesized from 1 μg of total RNA using a RevertAid First Strand cDNA Synthesis kit (Fermentas, Burlington, Canada). Next, qRT-PCR was performed using a FastStart Universal SYBR Premix ExTaq II (Takara Biotechnology, Japan) on an ABI PRISM 7900HT System (Applied Biosystems, Foster City, CA, USA). Relative gene expression was calculated via the $2^{-\triangle\triangle CT}$ method and GAPDH was used as the reference for normalization. The primer sequences used for qRT-PCR were as follows: FAK: forward, 5′-GAAGCATTGGGTCGG-GAACTA-3′, and reverse, 5′-CTCAATGCAGTTTGGAGGTGC-3′; GAPDH: forward, 5′-TGTCGTGGAGTCTACTGGTG-3′; and reverse, 5′-GCATTGCTGACAATCTTGAG-3′.

Western blotting (WB) and enzyme-linked immunosorbent assay (ELISA)

Proteins were collected as previously described from the cultured MSCs. The protein levels in the supernatant were measured using a Pierce BCA Protein Assay kit (Thermo Fisher Scientific, Waltham, MA, USA). We centrifuged the lysates and separated the supernatants via SDS-PAGE, blotted them onto polyvinylidene fluoride (PVDF) membranes (Bio-Rad Laboratories), analyzed them with specific antibodies for FAK (1:1000, sc-271195, Santa Cruz, Biotechnology, Heidelberg, Germany), p-FAK (1:1000, sc-374668, Santa Cruz, Biotechnology, Heidelberg, Germany), Grb2 (1:1000, PA5-27151, Thermo Fisher Scientific, Waltham, MA, USA), p-Grb2 (1:1000, Ser159, Thermo Fisher, Waltham, MA, USA), MAPK (1:1000, ab197348, Abcam, Cambridge, UK), p-MAPK (1:1000, CY6390, Abway, Beijing, China), and GAPDH (1:2000, 10494-1-AP, Proteintech, Wuhan, China), and visualized them via enhanced chemiluminescence (ECL kit, Amersham Biosciences). The concentrations of VEGF in the supernatant of the bone marrow, blood, or in the CM were measured using a commercial mouse VEGF ELISA kit (ab100751, Abcam, Cambridge, UK) according to the manufacturer's instructions. The optical density of each well was determined using a microplate reader (Bio-Rad 680, Hercules, CA, USA) set to 450 nm. Wavelength correction was set to 570 nm. The protein concentration in each sample was calculated according to the standard curve.

Statistical analysis

Data are presented as mean ± standard deviation (s.d). One-way analysis of variance (ANOVA) was used for multifactorial comparisons. First, homogeneity of variance was tested, after which differences between groups were assessed by post hoc multiple comparisons. If no

heterogeneity was observed, the LSD test was used to assess the differences between groups. However, if heterogeneity was present, the Welch test was used to determine the equality of means and Dunnett's T3 was used to assess the differences between groups. The investigators were blinded to allocations during the experiments and outcome assessment. In the figures, statistical significance is shown as follows: $*p < 0.05$, $**p < 0.01$ compared to sham, and $\#p < 0.05$, $\#\#p < 0.01$ compared to vehicle. All of the data analyses were conducted using SPSS 21.0 analysis software (SPSS Inc.).

Results

Defactinib inhibits the formation of H-type vessels in subchondral bone during OA pathogenesis

We previously found that elevated H-type vessels in subchondral bone correlating with osteoarthritis (OA) and focal adhesion kinase (FAK) in MSCs is critical for H-type vessel formation in osteoporosis [13,22]. In this study, we found that FAK expression was elevated significantly in the subchondral bone of the vehicle-treated ACLT mice in comparison with the sham controls and defactinib (FAK inhibitor)-treated ACLT mice (Fig. 1A). Through CT-based microangiography, we certified that the vessel number (VN) and vessel volume/total tissue volume (VV/TV) increased significantly in the subchondral bone of the vehicle-treated ACLT mice (Fig. 1B–D), whereas defactinib treatment normalized them. These demonstrated that the vasculature in the subchondral bone was significantly elevated during the onset of OA. We further confirmed that the increase in the vasculature was from H-type vessels. Double immunofluorescence staining of CD31 and endomucin revealed a significant increase in H-type vessels (CD31$^+$ endomucin$^+$) in the subchondral bone marrow of vehicle-treated ACLT mice, whereas defactinib treatment lowered H-type vessels with no significant difference relative to the sham controls (Fig. 1E and F). Taken together, these results demonstrate that an increase in FAK modulates H-type vessel formation during the onset of OA.
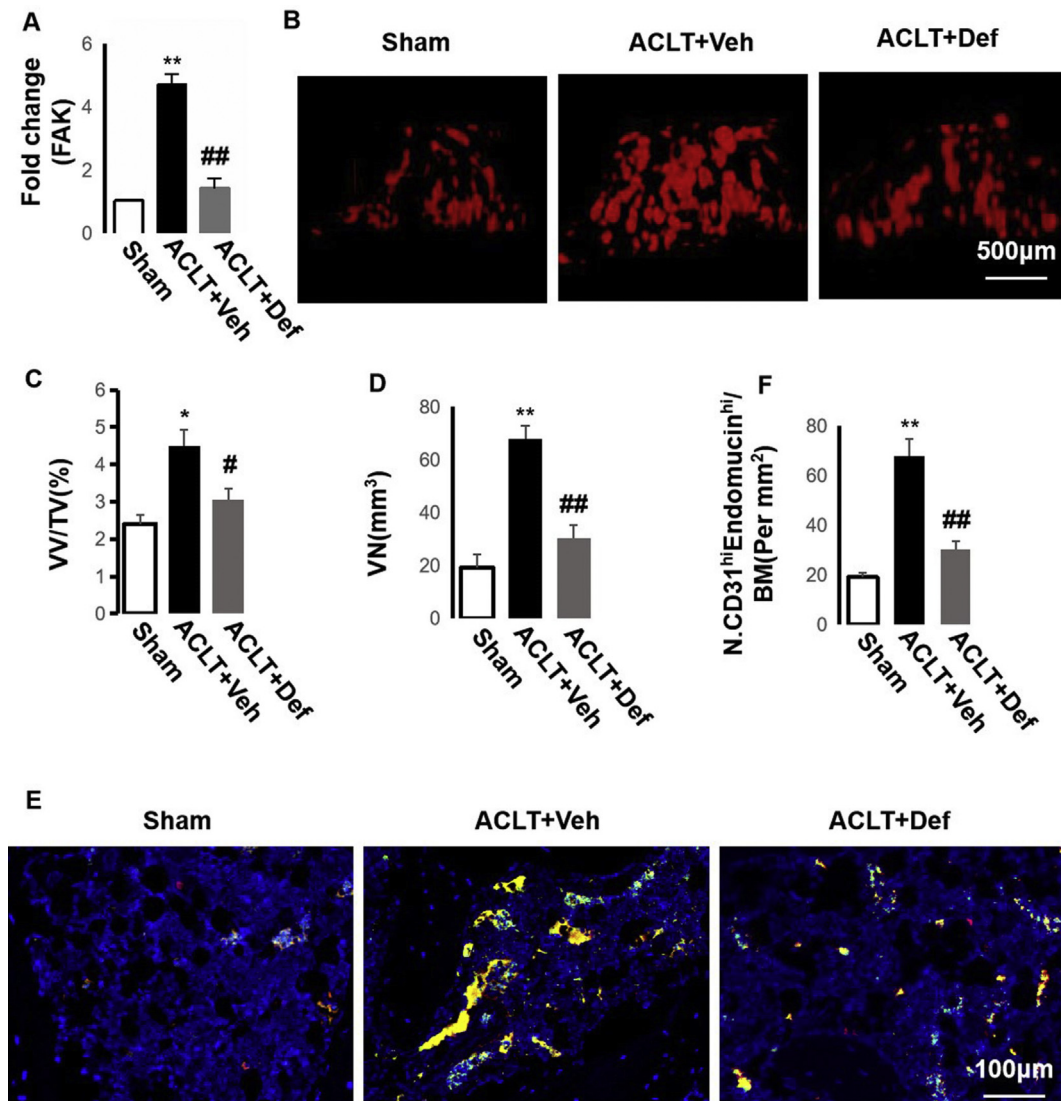

Fig. 1. Defactinib inhibits H-type vessels in subchondral bone. (A) qRT-PCR analysis of the mRNA expression of FAK in the subchondral bone. n = 5 per group. (B–D) Three-dimensional CT-based microangiography of the medial tibial subchondral bone one month post-surgery (B) with quantification of the vessel volume relative to the tissue volume (VV/TV) (C) and vessel number (VN) (D). n = 10 per group. Scale bar, 500 μm. (E–F) Confocal images (E) and quantification of CD31 and endomucin-positive cells (CD31: green; endomucin: red; merge: yellow). n = 10 per group. Scale bar, 100 μm. Sham = sham controls; ACLT + Veh = vehicle-treated ACLT mice; ACLT + Def = defactinib-treated ACLT mice. $*p < 0.05$ and $**p < 0.01$ compared to sham. $\#p < 0.05$ and $\#\#p < 0.01$ compared to vehicle.

Defactinib suppresses H-type vessel-induced abnormal bone formation in subchondral bone

H-type vessels couple angiogenesis with osteogenesis [16]. Triple immunofluorescence staining of CD31, endomucin, and Osterix revealed that elevated H-type vessels were highly enriched by Osterix-positive cells. Defactinib-treated ACLT mice had significantly decreased H-type vessels and accompanied Osterix⁺ cells, similar to the level of the sham
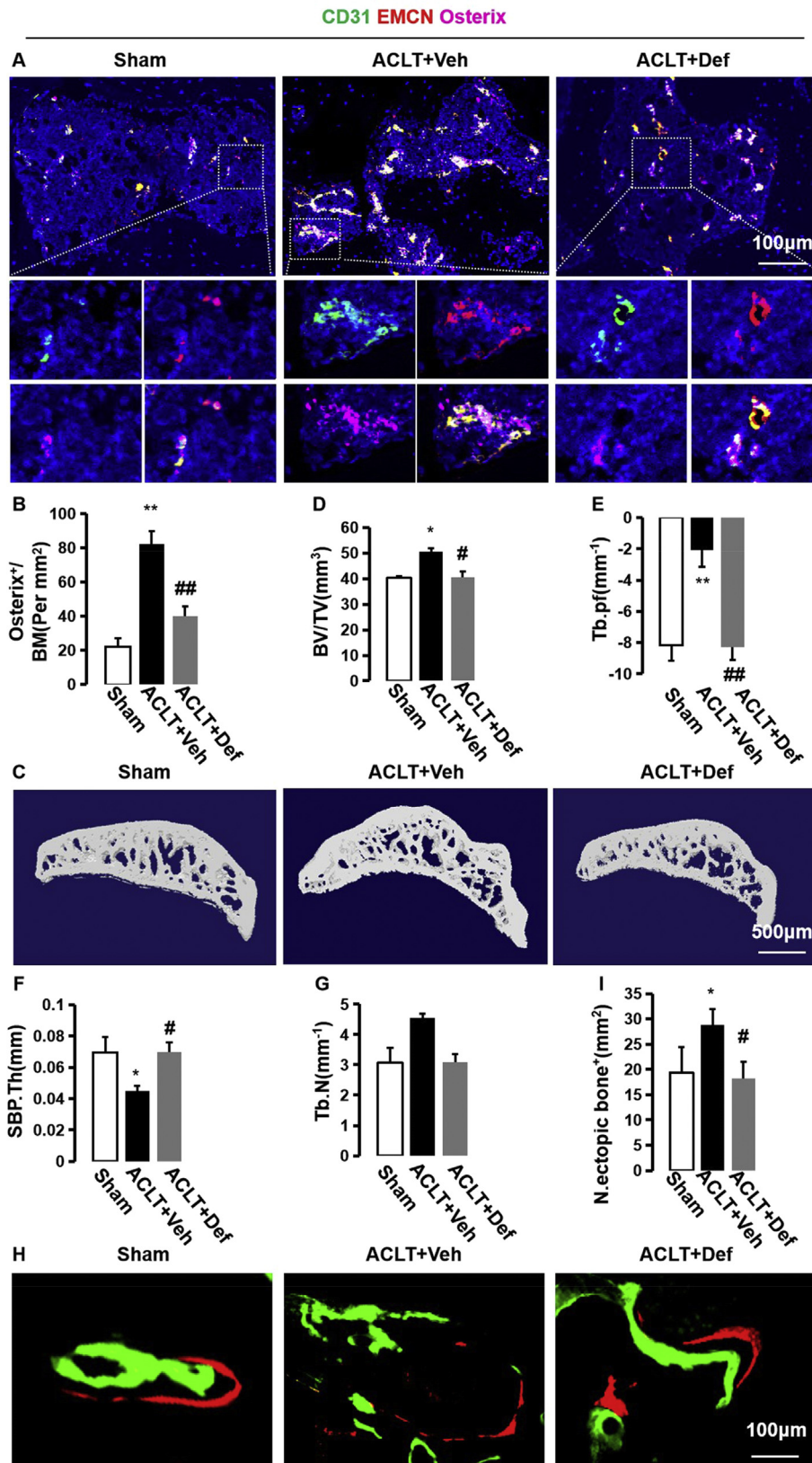

Fig. 2. Defactinib inhibits h-type vessel-induced abnormal bone formation in subchondral bone. (A and B) Confocal images (A) and quantification of CD31 and endomucin-positive cells (CD31: green; endomucin: red; merge: yellow) and Osterix⁺ (purple) cells. n = 10 per group. Scale bar, 100 μm. (C) Representative three-dimensional micro-CT images of the sagittal views of the subchondral bone medial compartment. Scale bar, 500 μm. (D–G) Quantitative micro-CT analysis of the tibial subchondral bone of the bone tissue relative to the total tissue volume (BV/TV). (D) Trabecular pattern factor (Tb.pf). (E) Subchondral bone plate thickness (SBP.Th). (F) Trabecular N (Tb.N) (G). n = 10 per group. (H) Fluorochromes xylenol orange and calcein green staining in the subchondral bone after surgery. Scale bar, 100 μm. (I) Quantification of abnormal bone formation in the subchondral bone. n = 5 per group. Sham = sham controls; ACLT + Veh = vehicle-treated ACLT mice; ACLT + Def = Defactinib-treated ACLT mice. *p < 0.05 and **p < 0.01 compared to sham. #p < 0.05 and ##p < 0.01 compared to vehicle.

controls (Fig. 2A and B). This implies that H-type vessels are strongly correlated with abnormal bone formation in subchondral bone. To detect the changes in the subchondral bone microarchitecture, we then performed three-dimensional microcomputed tomography (μCT) of the tibial subchondral bone and found increased BV/TV and Tb.Pf and reduced SBP thickness in the vehicle-treated ACLT mice. Defactinib treatment, however, normalized BV/TV, Tb.Pf, and SBP.Th with no significant difference noted relative to the sham controls (Fig. 2C–G). In addition, fluorescent double-labeling experiments revealed that abnormal bone formation in the subchondral bone was enhanced in the vehicle-treated ACLT mice (green and orange were not linked and separated from each other) relative to the sham controls (green and orange were layered and closer to each other), whereas defactinib treatment decreased abnormal bone formation in the subchondral bone (Fig. 2H and I). Taken together, these results suggest that elevated H-type vessels link abnormal bone formation in subchondral bone during the onset of OA.

Defactinib further protects articular cartilage from degeneration

Abnormal bone formation in subchondral bone can result in subsequent articular cartilage degradation [8,9,11–13]. Safranin O/fast green staining revealed that proteoglycan loss was significantly alleviated in the defactinib-treated ACLT mice compared with the vehicle-treated ACLT mice, similar to the level of the sham controls (Fig. 3A). Osteoarthritis Research Society International (OARSI)-modified Mankin scores also showed that defactinib treatment significantly lowered OARSI scores compare to the vehicle-treated ACLT mice (Fig. 3B). Additionally, HE staining showed that defactinib treatment rescued the thickening of calcified cartilage zone defined by an upward moving tidemark in the vehicle-treated ACLT mice (Fig. 3C and D). Moreover, immunofluorescence staining of the cartilage markers revealed increased MMP13 and ADAMTS5 and decreased collagen II and aggrecan in the vehicle-treated ACLT mice. Treatment with defactinib normalized the expression of MMP13, ADAMTS5, collagen II, and aggrecan in the cartilage similar to the sham controls (Fig. 3E–I). Combined with in Figs. 1 and 2, these results demonstrate that defactinib may protect articular cartilage from degeneration through the inhibition of H-type vessel-induced abnormal bone formation in the subchondral bone.

Defactinib lowers H-type vessel-linked MSCs essential for abnormal bone formation in subchondral bone

Abnormal bone formation results from erroneous mobilization and recruitment of MSCs to bone marrow cavities or non-bone resorption sites but not to bone resorption pits [12,29]. We explored whether inhibition of H-type vessels with defactinib could reduce MSCs in subchondral bone. Fluorescence-activated cell sorting (FACS) was used to sort MSCs (CD45$^-$CD29$^+$Sca-1$^+$CD105$^+$) from subchondral bone in the sham controls, vehicle-treated ACLT mice, and defactinib-treated ACLT mice. The results showed that the amount of MSCs increased dramatically in the subchondral bone of the vehicle-treated ACLT mice. Treatment with defactinib significantly reduced the amount of MSCs in the subchondral bone, with no significant difference noted relative to the sham controls (Fig. 4A and B). Immunofluorescence staining of nestin revealed similar results (Fig. 4C and D). We further revealed that H-type vessels in the subchondral bone were highly enriched by CD146$^+$ perivascular cells [30–32], whereas defactinib treatment reduced H-type vessels and accompanied CD146$^+$ perivascular cells, similar to the level of the sham controls (Fig. 4E–G). Taken together, these results indicate that H-type vessels might be integral to the origin of MSCs necessary for abnormal bone formation in subchondral bone during OA progression.

Defactinib further inhibits MSC-regulated angiogenesis

To investigate the role of subchondral bone MSCs in the different

groups on angiogenesis, we first cultured MSCs from subchondral bone of the groups. We previously found that FAK activation in MSCs enhanced H-type vessel formation in cortical bone to alleviate osteoporosis [22]. Thus, we performed immunofluorescence staining of p-FAK in MSCs from the different groups and revealed that p-FAK in MSCs from the vehicle-treated ACLT mice was higher than those from the sham controls and defactinib-treated ACLT mice (Fig. 5A and B). Western blotting confirmed that defactinib inhibited activation of FAK and further exerted an effect on the FAK-Grb2-MAPK pathway (Fig. 5C and D).

FAK signaling can modulate angiogenesis through FAK-Grb2-MAPK-linked VEGF expression [24]. We then detected the level of VEGF in the CM of the MSCs from the different groups and found that its level in the CM of the MSCs from the vehicle-treated ACLT mice was higher than in the sham controls and defactinib-treated ACLT mice. This was similar to the VEGF level in subchondral bone and blood *in vivo* (Fig. 6A–C). We then investigated the effect of the CM of MSCs on the angiogenesis of ECs *in vitro*. We divided the CM into four groups according to the source of MSCs: sham controls, vehicle-treated ACLT mice, vehicle-treated ACLT mice with the addition of VEGF neutralizing antibody in CM, and defactinib-treated ACLT mice. We found that the CM of the MSCs from the vehicle-treated ACLT mice promoted angiogenesis of ECs, whereas the addition of VEGF neutralizing antibody in the CM of the MSCs from the vehicle-treated mice and defactinib-treated ACLT mice significantly decreased angiogenesis of ECs similar to the CM of the MSCs from the sham controls (Fig. 6D–G). Taken together, these results demonstrate that subchondral bone MSCs can enhance angiogenesis through FAK-Grb2-MAPK-linked VEGF expression.

Discussion

Subchondral bone and overlying articular cartilage form functional units in the joints [8,9]. Subchondral bone provides mechanical support for overlying articular cartilage and undergoes constant remodeling to adapt to changes in the surrounding mechanical environment. It has been reported that changes in subchondral bone precede articular cartilage during OA pathogenesis [33–35]. Abnormal bone formation exerts a key role in the degeneration of articular cartilage [12]. Specifically, under normal conditions, subchondral bone undergoes coupled bone remodeling to maintain the homeostasis and structure integrity of the overlying cartilage. However, following an acute injury of joint instability, increased and uncoupled bone remodeling occurs, resulting in a varied metabolic microenvironment beneficial for angiogenesis and abnormal osteogenesis in subchondral bone. Of note, abnormal bone formation is mainly involved in the subchondral plate and calcified cartilage [9], key regions of initial cartilage degeneration. Moreover, articular cartilage is designed for loadbearing, and cartilage's high water allows it to deform without failure under compressive loads. However, cartilage is mechanically less capable of withstanding tension or shear stresses [9]. Thus, regions with abnormal bone formation in the junction of the subchondral plate and calcified cartilage cause cartilage to deform more, leading to cartilage degeneration. It has been reported recently that orchestration of increased subchondral bone remodeling using bisphosphonate (BP) therapy in patients with knee OA attenuated OA progression and decreased the risk of knee replacement surgery [36,37]. In this study, we also found that the inhibition of H-type vessels in subchondral bone could alleviate overlying cartilage degeneration and attenuate the onset of OA.

Osteogenesis is often coupled with angiogenesis [38]. H-type vessels, a recently identified specific vessel subtype, link angiogenesis with osteogenesis [16,17]. This study demonstrated that H-type vessels were strongly correlated with abnormal bone formation in OA pathogenesis. Triple immunofluorescence staining showed that H-type vessels were highly enriched by Osterix-positive cells. Inhibition of H-type vessels in subchondral bone significantly inhibited the amount of accompanied Osterix-positive cells. Micro-CT and calcein double-labeling experiments confirmed that the inhibition of H-type vessels reduced abnormal bone
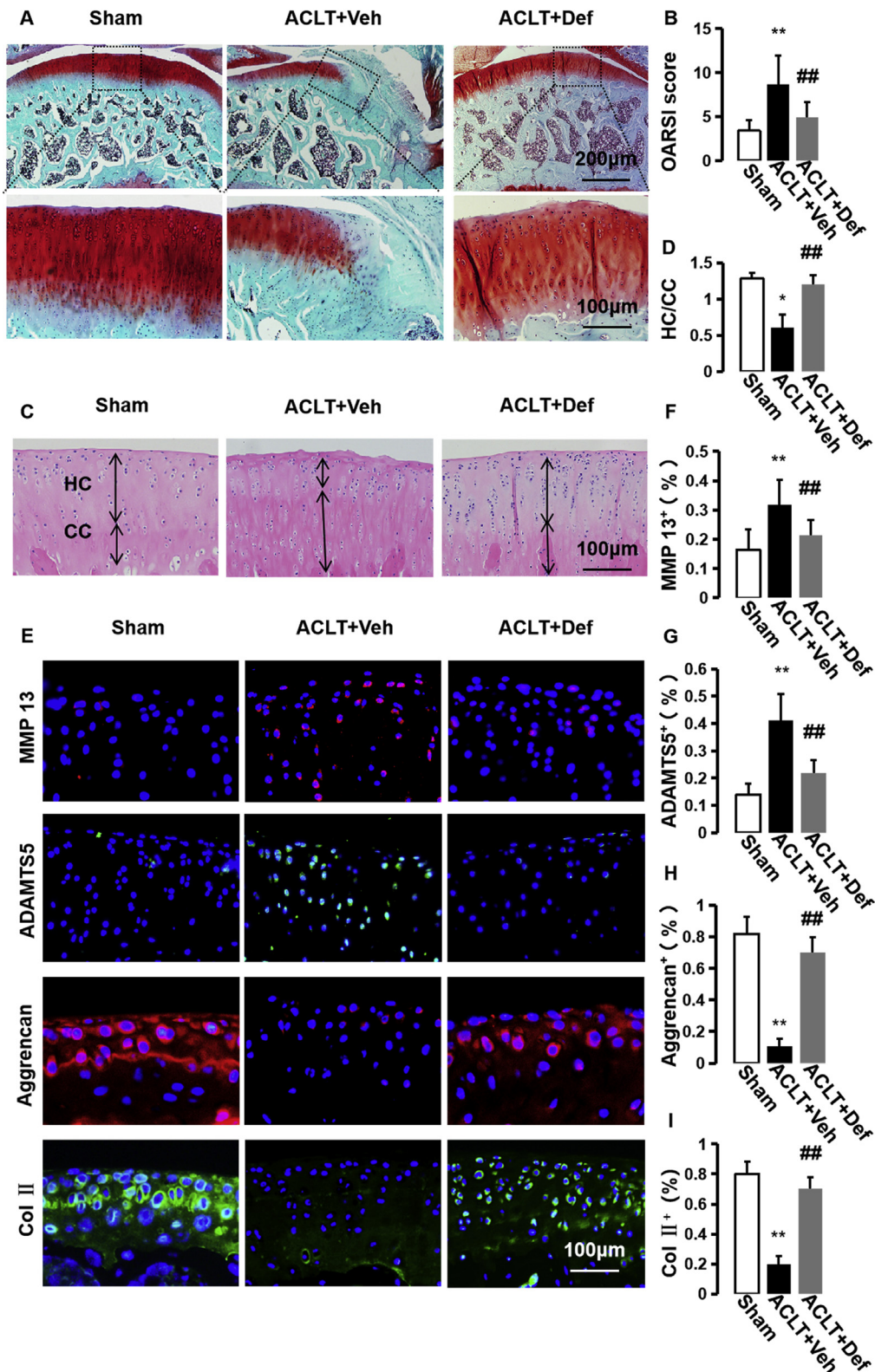
Fig. 3. Defactinib further protects articular cartilage from degeneration. (A) Safranin O and fast green staining (top). Scale bar, 200 μm. Magnified view (bottom) of Safranin O and fast green staining. Scale bar, 100 μm. (B) International modified Mankin scores of articular cartilage 60 days after surgery. n = 10 per group. (C) H&E staining where double-headed arrows mark calcified cartilage (CC) and hyaline cartilage (HC) thickness. Scale bars, 100 μm. (D) Quantitative analysis of HC/CC ratio in cartilage. n = 10 per group. (E–I) Immunostaining and quantification of MMP-13, ADAMTS 5, Aggrecan, and Col II in articular cartilage 60 days post-operation. n = 10 per group. Scale bar, 100 μm. Sham = sham controls; ACLT + Veh = vehicle-treated ACLT mice; ACLT + Def = defactinib-treated ACLT mice. *$p < 0.05$ and **$p < 0.01$ compared to sham. #$p < 0.05$ and ##$p < 0.01$ compared to vehicle.
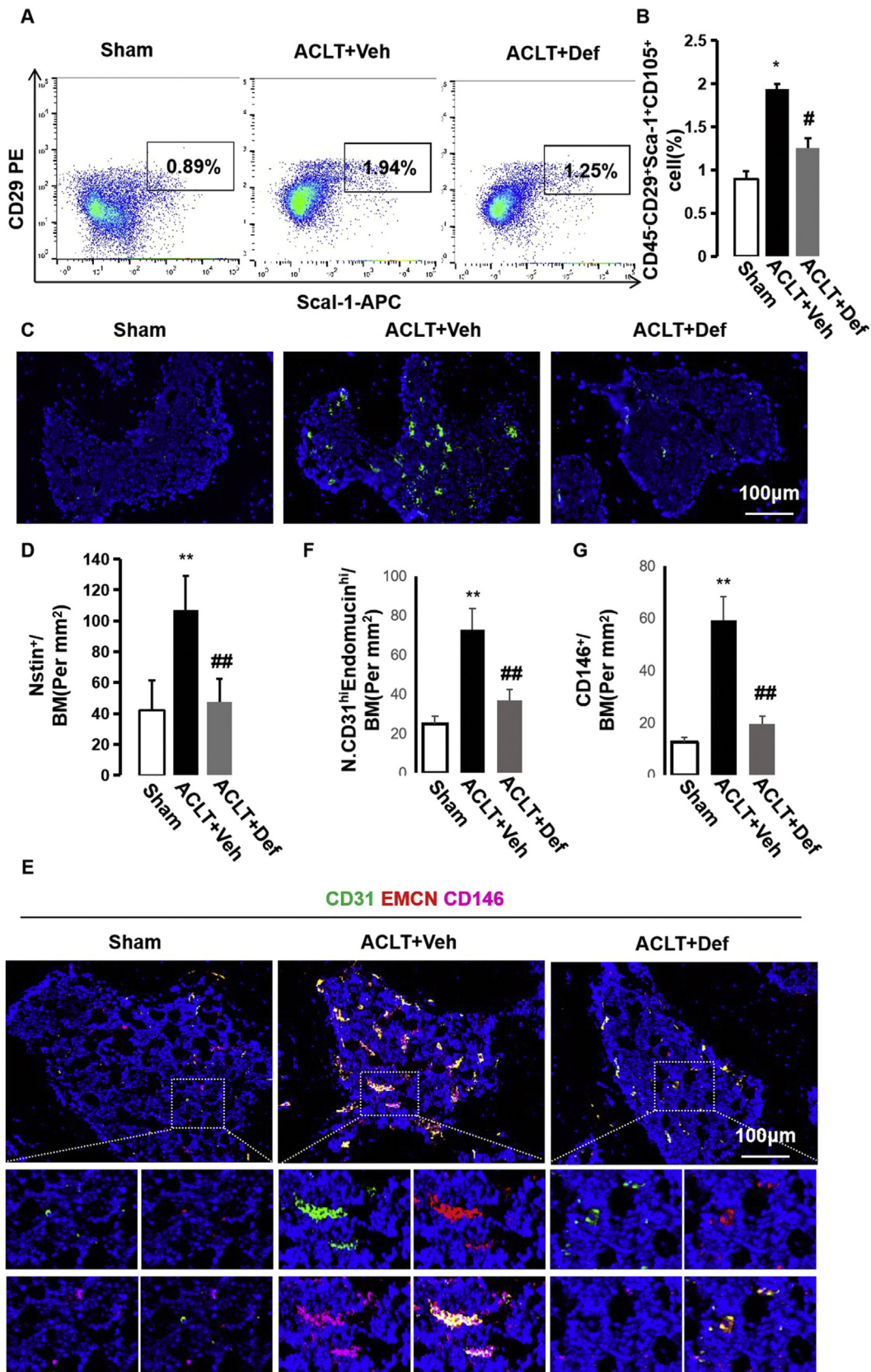
Fig. 4. Defactinib lowers H-type vessel-linked MSCs in subchondral bone. (A and B) Representative images of flow cytometry (A) and quantification of the percentages of MSCs (CD29$^+$CD90$^+$CD45$^-$) (B) isolated from the subchondral bone of the sham controls, vehicle-treated ACLT mice, and defactinib-treated ACLT mice. n = 5 per group. (C and D) Immunostaining and quantification of nestin-positive cells in the subchondral bone of the different groups. Scale bar, 100 μm. (E–G) Confocal images and quantification of CD31 and endomucin-positive cells (CD31: green; endomucin: red; merge: yellow) and CD146$^+$ (purple) cells. n = 10 per group. Scale bar, 100 μm. Sham = sham controls; ACLT + Veh = vehicle-treated ACLT mice; ACLT + Def = defactinib-treated ACLT mice. *p < 0.05 and **p < 0.01 compared to sham. #p < 0.05 and ##p < 0.01 compared to vehicle.
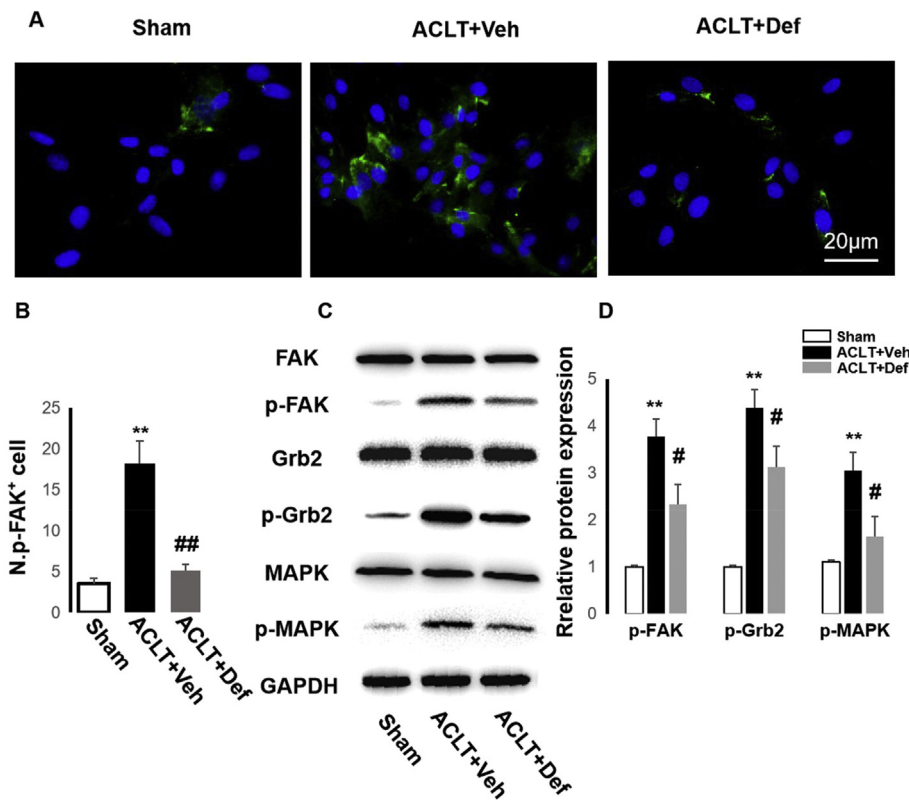
Fig. 5. Defactinib inhibits the activation of FAK-Grb2-MARK in MSCs from subchondral bone during OA development. (A and B) Immunostaining and quantification of p-FAK in MSCs from subchondral bone of the sham controls, vehicle-treated ACLT mice, and defactinib-treated ACLT mice. Scale bar, 20 μm n = 5 per group. (C and D) Western blotting of p-FAK, p-Grb2, and p-MAPK in MSCs from the different groups. Sham = sham controls; ACLT + Veh = vehicle-treated ACLT mice; ACLT + Def = defactinib-treated ACLT mice. *p < 0.05 and **p < 0.01 compared to sham. #p < 0.05 and ##p < 0.01 compared to vehicle.
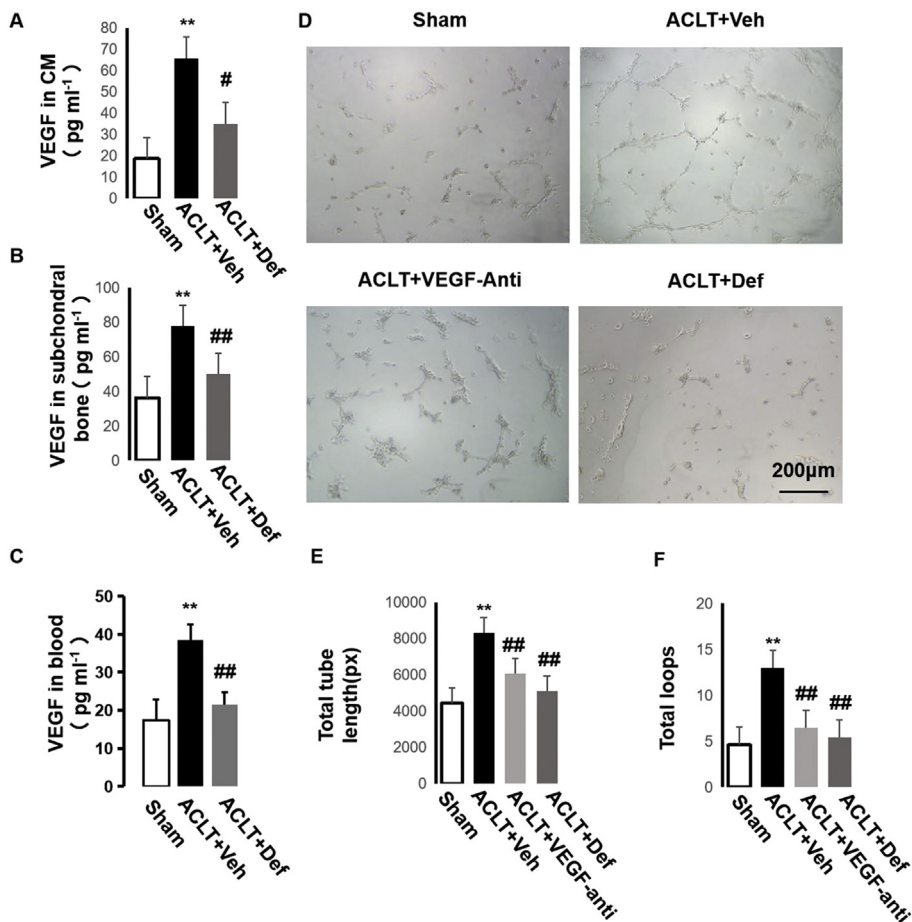

Fig. 6. Defactinib inhibits MSC-regulated angiogenesis through FAK-Grb2-MAPK-linked VEGF. (A–C) ELISA analysis of the expression of VEGF in CM of MSCs from the different groups (A), subchondral bone marrow (B), and in blood (C). n = 5 per group. (D) Representative images showing tube formation of BMECs on Matrigel. Scale bar: 200 μm. (E–F) Total tube length and total loops were measured to quantify the ability of BMECs to form tubes. n = 5 per group. Sham = CM of MSCs from the sham controls; ACLT + Veh = CM of MSCs from the vehicle-treated ACLT mice; ACLT + Def = CM of MSCs from the defactinib-treated ACLT mice; ACLT + VEGF-anti = addition of VEGF neutralizing antibody in CM of MSCs from the vehicle-treated ACLT mice. *p < 0.05 and **p < 0.01 compared to sham. #p < 0.05, ##p < 0.01 compared to vehicle.

formation in subchondral bone. Flow cytometry results revealed that the amount of MSCs in the defactinib-treated ACLT mice dramatically decreased in comparison with the vehicle-treated ACLT mice. We found that H-type vessels were highly surrounded by CD146$^+$ perivascular cells [30–32], whereas defactinib treatment significantly inhibited H-type vessels and accompanying CD146$^+$ perivascular cells.

MSCs are believed to reside as perivascular cells or pericytes. In 2008, Crisan et al. first reported that pericytes expressed MSC marks *in vivo* and behaved as MSCs *in vitro*, which was a prominent advance toward the identification of MSCs [39]. Since then, increasing studies have advocated this concept, demonstrating that transplantation of purified pericytes [31,39] and genetically traced pericytes [40–42] may lead to tissue-specific repair *in vivo*. However, one important question yet to be answered is whether all pericytes function equally, as some opposing viewpoints have proposed [43]. We posit that pericytes may behave as MSCs but that this behavior depends on the specific tissues and developmental stages [44,45]. Combined with our results, we believe that H-type vessels, elevated in subchondral bone during OA progression, might be integral to the origin of the elusive MSCs necessary for aberrant bone formation.

In turn, MSCs further enhance angiogenesis to form a positive feedback loop between H-type vessels and MSCs. We previously found that FAK activation in MSCs promoted H-type vessel formation in osteoporosis [22]. However, it remains unknown whether this is suitable for OA development. We isolated MSCs from the subchondral bone of sham controls, vehicle-treated ACLT mice, and defactinib-treated ACLT mice to explore the role of subchondral bone MSCs on angiogenesis. We found that p-FAK was increased significantly in the MSCs from the vehicle-treated ACLT mice in comparison with the sham controls and defactinib-treated ACLT mice. Moreover, the CM of the MSCs from the vehicle-treated ACLT mice enhanced angiogenesis of ECs *in vitro*, whereas the addition of VEGF neutralizing antibody in the CM of the MSCs from the vehicle-treated mice and defactinib-treated ACLT mice significantly inhibited angiogenesis of ECs.

Conclusions

Taken together, our present study revealed that, during OA pathogenesis, H-type vessels and MSCs formed a positive feedback loop contributing to abnormal bone formation in subchondral bone. H-type vessels provide MSCs integral to abnormal bone formation during OA progression, and MSCs in turn enhance angiogenesis through the FAK-Grb2-MAPK pathway. Further, defactinib can attenuate OA by inhibiting H-type vessel-linked MSCs indispensable to abnormal bone formation in subchondral bone.

Funding information

Conflict of Interest

The authors have no conflicts of interest to disclose in relation to this article.

References

[1] Gregori D, Giacovelli G, Minto C, Barbetta B, Gualtieri F, Azzolina D, et al. Association of pharmacological treatments with long-term pain control in patients with knee osteoarthritis: a systematic review and meta-analysis. JAMA 2018; 320(24):2564–79.

[2] Lawrence RC, Felson DT, Helmick CG, Arnold LM, Choi H, Deyo RA, et al. Estimates of the prevalence of arthritis and other rheumatic conditions in the United States. Part II. Arthritis Rheum 2008;58(1):26–35.

[3] Berenbaum F, Wallace IJ, Lieberman DE, Felson DT. Modern-day environmental factors in the pathogenesis of osteoarthritis. Nat Rev Rheumatol 2018;14(11): 674–81.

[4] Collins NJ, Hart HF, Mills KAG. Osteoarthritis year in review 2018: rehabilitation and outcomes. Osteoarthritis Cartilage 2019;27(3):378–91.

[5] Khorasani MS, Diko S, Hsia AW, Anderson MJ, Genetos DC, Haudenschild DR, et al. Effect of alendronate on post-traumatic osteoarthritis induced by anterior cruciate ligament rupture in mice. Arthritis Res Ther 2015;17:30.

[6] Cui Z, Xu C, Li X, Song J, Yu B. Treatment with recombinant lubricin attenuates osteoarthritis by positive feedback loop between articular cartilage and subchondral bone in ovariectomized mice. Bone 2015;74:37–47.

[7] Roman-Blas JA, Herrero-Beaumont G. Targeting subchondral bone in osteoporotic osteoarthritis. Arthritis Res Ther 2014;16(6):494.

[8] Lories RJ, Luyten FP. The bone-cartilage unit in osteoarthritis. Nat Rev Rheumatol 2011;7(1):43–9.

[9] Burr DB, Gallant MA. Bone remodelling in osteoarthritis. Nat Rev Rheumatol 2012; 8(11):665–73.

[10] Goldring SR. Alterations in periarticular bone and cross talk between subchondral bone and articular cartilage in osteoarthritis. Ther Adv Musculoskelet Dis 2012; 4(4):249–58.

[11] Shen J, Li S, Chen D. TGF-beta signaling and the development of osteoarthritis. Bone Res 2014;2:14002.

[12] Zhen G, Wen C, Jia X, Li Y, Crane JL, Mears SC, et al. Inhibition of TGF-beta signaling in mesenchymal stem cells of subchondral bone attenuates osteoarthritis. Nat Med 2013;19(6):704–12.

[13] Cui Z, Crane J, Xie H, Jin X, Zhen G, Li C, et al. Halofuginone attenuates osteoarthritis by inhibition of TGF-beta activity and H-type vessel formation in subchondral bone. Ann Rheum Dis 2016;75(9):1714–21.

[14] Percival CJ, Richtsmeier JT. Angiogenesis and intramembranous osteogenesis. Dev Dyn 2013;242(8):909–22.

[15] Chim SM, Tickner J, Chow ST, Kuek V, Guo B, Zhang G, et al. Angiogenic factors in bone local environment. Cytokine Growth Factor Rev 2013;24(3):297–310.

[16] Kusumbe AP, Ramasamy SK, Adams RH. Coupling of angiogenesis and osteogenesis by a specific vessel subtype in bone. Nature 2014;507(7492):323–8.

[17] Ramasamy SK, Kusumbe AP, Wang L, Adams RH. Endothelial Notch activity promotes angiogenesis and osteogenesis in bone. Nature 2014;507(7492):376–80.

[18] Carmeliet P, Jain RK. Molecular mechanisms and clinical applications of angiogenesis. Nature 2011;473(7347):298–307.

[19] Chen WC, Park TS, Murray IR, Zimmerlin L, Lazzari L, Huard J, et al. Cellular kinetics of perivascular MSC precursors. Stem Cells Int 2013;2013:983059.

[20] Bronckaers A, Hilkens P, Martens W, Gervois P, Ratajczak J, Struys T, et al. Mesenchymal stem/stromal cells as a pharmacological and therapeutic approach to accelerate angiogenesis. Pharmacol Ther 2014;143(2):181–96.

[21] Nassiri SM, Rahbarghazi R. Interactions of mesenchymal stem cells with endothelial cells. Stem Cells Dev 2014;23(4):319–32.

[22] Xie H, Cui Z, Wang L, Xia Z, Hu Y, Xian L, et al. PDGF-BB secreted by preosteoclasts induces angiogenesis during coupling with osteogenesis. Nat Med 2014;20(11): 1270–8.

[23] Zhao X, Guan JL. Focal adhesion kinase and its signaling pathways in cell migration and angiogenesis. Adv Drug Deliv Rev 2011;63(8):610–5.

[24] Mitra SK, Mikolon D, Molina JE, Hsia DA, Hanson DA, Chi A, et al. Intrinsic FAK activity and Y925 phosphorylation facilitate an angiogenic switch in tumors. Oncogene 2006;25:5969–84.

[25] Kang Y, Hu W, Ivan C, Dalton HJ, Miyake T, Pecot CV, et al. Role of focal adhesion kinase in regulating YB-1-mediated paclitaxel resistance in ovarian cancer. J Natl Cancer Inst 2013;105(19):1485–95.

[26] Pritzker KP, Gay S, Jimenez SA, Ostergaard K, Pelletier JP, Revell PA, et al. Osteoarthritis cartilage histopathology: grading and staging. Osteoarthritis Cartilage 2006;14(1):13–29.

[27] Siclari VA, Zhu J, Akiyama K, Liu F, Zhang X, Chandra A, et al. Mesenchymal progenitors residing close to the bone surface are functionally distinct from those in the central bone marrow. Bone 2013;53(2):575–86.

[28] Yao Z, Chen P, Wang S, Deng G, Hu Y, Lin Q, et al. Reduced PDGF-AA in subchondral bone leads to articular cartilage degeneration after strenuous running. J Cell Physiol 2019;234(10):17946–58.

[29] Supakul S, Yao K, Ochi H, Shimada T, Hashimoto K, Sunamura S, et al. Pericytes as a source of osteogenic cells in bone fracture healing. Int J Mol Sci 2019;20(5): E1079.

[30] Chen J, Luo Y, Hui H, Cai T, Huang H, Yang F, et al. CD146 coordinates brain endothelial cell-pericyte communication for blood-brain barrier development. Proc Natl Acad Sci U S A 2017;114(36):E7622–31.

[31] Chen WC, Baily JE, Corselli M, Diaz ME, Sun B, Xiang G, et al. Human myocardial pericytes: multipotent mesodermal precursors exhibiting cardiac specificity. Stem Cell 2015;33(2):557–73.

[32] Crisan M, Yap S, Casteilla L, Chen CW, Corselli M, Park TS, et al. A perivascular origin for mesenchymal stem cells in multiple human organs. Cell Stem Cell 2008; 3(3):301–13.

[33] Raynauld JP, Martel-Pelletier J, Berthiaume MJ, Abram F, Choquette D, Haraoui B, et al. Correlation between bone lesion changes and cartilage volume loss in patients with osteoarthritis of the knee as assessed by quantitative magnetic resonance imaging over a 24-month period. Ann Rheum Dis 2008;67(5):683–8.

[34] Roemer FW, Guermazi A, Javaid MK, Lynch JA, Niu J, Zhang Y, et al. Change in MRI-detected subchondral bone marrow lesions is associated with cartilage loss: the

MOST Study. A longitudinal multicentre study of knee osteoarthritis. Ann Rheum Dis 2009;68(9):1461–5.

[35] Tanamas SK, Wluka AE, Pelletier JP, Pelletier JM, Abram F, Berry PA, et al. Bone marrow lesions in people with knee osteoarthritis predict progression of disease and joint replacement: a longitudinal study. Rheumatology (Oxford) 2010;49(12): 2413–9.

[36] Fu SH, Wang CY, Yang RS, Wu FL, Hsiao FY. Bisphosphonate use and the risk of undergoing total knee arthroplasty in osteoporotic patients with osteoarthritis: a nationwide cohort study in Taiwan. J Bone Joint Surg Am 2017;99(11):938–46.

[37] Neogi T, Li S, Peloquin C, Misra D, Zhang Y. Effect of bisphosphonates on knee replacement surgery. Ann Rheum Dis 2018;77(1):92–7.

[38] Portal-Nunez S, Lozano D, Esbrit P. Role of angiogenesis on bone formation. Histol Histopathol 2012;27(5):559–66.

[39] Dellavalle A, Sampaolesi M, Tonlorenzi R, Tagliafico E, Sacchetti B, Perani L, et al. Pericytes of human skeletal muscle are myogenic precursors distinct from satellite cells. Nat Cell Biol 2007;9(3):255–67.

[40] Feng J, Mantesso A, De Bari C, Nishiyama A, Sharpe PT. Dual origin of mesenchymal stem cells contributing to organ growth and repair. Proc Natl Acad Sci U S A 2011;108(16):6503–8.

[41] Krautler NJ, Kana V, Kranich J, Tian Y, Perera D, Lemm D, et al. Follicular dendritic cells emerge from ubiquitous perivascular precursors. Cell 2012;150(1):194–206.

[42] Tang W, Zeve D, Suh JM, Bosnakovski D, Kyba M, Hammer RE, et al. White fat progenitor cells reside in the adipose vasculature. Science 2008;322(5901):583–6.

[43] Guimaraes-Camboa N, Cattaneo P, Sun Y, Moore-Morris T, Gu Y, Dalton ND, et al. Pericytes of multiple organs do not behave as mesenchymal stem cells in vivo. Cell Stem Cell 2017;20(3):345–359 e5.

[44] Cano E, Gebala V, Gerhardt H. Pericytes or mesenchymal stem cells: is that the question? Cell Stem Cell 2017;20(3):296–7.

[45] Fiedler J, Etzel N, Brenner RE. To go or not to go: migration of human mesenchymal progenitor cells stimulated by isoforms of PDGF. J Cell Biochem 2004;93(5):990–8.